# A Novel Role of FoxO3a in the Migration and Invasion of Trophoblast Cells: From Metabolic Remodeling To Transcriptional Reprogramming

**Hao Chen**
The First Affiliated Hospital of Chongqing Medical University
**Shi-Han Wang**
The First Affiliated Hospital of Chongqing Medical University
**Chang Chen**
The First Affiliated Hospital of Chongqing Medical University
**Xin-Yang Yu**
The First Affiliated Hospital of Chongqing Medical University
**Jia-Nan Zhu**
The First Affiliated Hospital of Chongqing Medical University
**Toby Mansell**
Murdoch Childrens Research Institute
**Boris Novakovic**
Murdoch Childrens Research Institute
**Richard Saffery**
Murdoch Childrens Research Institute
**Philip N. Baker**
University of Leicester
**Ting-Li Han**
The Second Affiliated Hospital of Chongqing Medical University
**Hua Zhang** ( zh2844@gmail.com )
The First Affiliated Hospital of Chongqing Medical University https://orcid.org/0000-0003-3501-8385

**Research Article**

**Keywords:** Preeclampsia, forkhead box O3a protein, aromatic amino acid, long-chain unsaturated fatty acid, migration

**Posted Date:** January 19th, 2022

**DOI:** https://doi.org/10.21203/rs.3.rs-1221183/v1

## Abstract

# Background

The forkhead box O3a protein (FoxO3a) has been reported to involve in the migration and invasion, but their underlying mechanisms in the trophoblast remain unknown. In this study, we aim to explore the transcriptional and metabolic regulations of FoxO3a on the migration and invasion of early placental development.

# Methods

Lentiviral vectors were used to knock down the expression of FoxO3a of the HTR8/SVneo cells. Western blot, matrigel invasion assay, wound healing assay, seahorse, gas-chromatography-mass spectrometry (GC-MS) based metabolomics, fluxomics, and RNA-seq transcriptomics were performed.

# Results

We found that FoxO3a depletion restrained the migration and invasion of HTR8/SVneo cells. Metabolomics, fluxomics, and seahorse demonstrated that FoxO3a knockdown resulted in a switch from aerobic to anaerobic respiration and increased utilization of aromatic amino acids and long-chain fatty acids from extracellular nutrients. Furthermore, our RNA-seq also demonstrated that the expression of COX-2 and MMP9 decreased after FoxO3a knockdown, and these two genes were closely associated with the migration/invasion progress of trophoblast cells.

# Conclusions

Our results suggested novel biological roles of FoxO3a in early placental development. FoxO3a exerts an essential effect on trophoblast migration and invasion owing to the regulations of COX2, MMP9, aromatic amino acids, energy metabolism, and oxidative stress.

## Background

Dysfunctional placentation increases the risk of adverse outcomes of mother and fetus in late gestation (Yang et al. 2017). In the early stage of vascular recasting, trophoblasts invade the spiral artery wall, and vascular endothelial cells are gradually replaced by trophoblast cells (Brosens et al. 2011; Burton et al. 2002; Xu et al. 2018). These allow the vascular cavity to expand, and subsequently, enlarged vascular diameter enables the adequate blood flow and perfusion of the placenta (Yang et al. 2017). Once dysfunction of trophoblast cells appears, it will cause vascular remodeling disorder and superficial invasion, which results in placental dysplasia. Especially, placental disorders may increase the likelihood

of preeclampsia (PE), fetal growth restriction (FGR), and recurrent miscarriage in pregnant women (Brosens et al. 2011; Hemberger et al. 2020).

The forkhead box O3a (FoxO3a), which is a member of the forkhead protein factor family (Foxes) (Zaheer et al. 2007), is widely expressed in different tissues and organs, including the heart, placenta, vascular endothelium, and fat (Hedrick et al. 2012; Zhang et al. 2006). FoxO3a involves many cell biological processes, such as cell migration, invasion, metabolism, autophagy, anti-oxidative stress, and apoptosis (CarlssonMahlapuu 2002; Warr et al. 2013). There was evidence that FoxO3a promoted the activity of gene networks involved in long-chain fatty acids biosynthesis and catabolism to promote longevity by cooperating with other transcription factors at the level of gene promoter (Amrit et al. 2016; Dansen et al. 2004). Furthermore, It has been reported that long-chain fatty acids, especially the arachidonic acid (AA), were associated with migration and invasion of cancer (Szymczak et al. 2008). Cyclooxygenase-2 (COX-2) is excessively expressed in many human carcinomas and converts the AA to prostaglandin E2 (PGE2), which promotes metastasis of tumors (Cui et al. 2012). On the other hand, increasing evidence illustrated the inseparable correlation between amino acids and cancer metastasis (Hasim et al. 2013; Hasim et al. 2012). Aromatic amino acids are related to COX-2-mediated migration and invasion (Cheng et al. 2012; Gu et al. 2021). Although many studies pinpoint that FoxO3a plays an essential regulatory role in long-chain fatty acids and amino acids metabolism, the potential mechanism of how FoxO3a modulates these metabolites to mediate trophoblast migration and invasion remains unknown.

Hence, the purpose of this study is to investigate the role of FoxO3a in the HTR8/SVneo cell line and the related mechanism on long-chain fatty acids and amino acids metabolism that are associated with migration and invasion, hoping to understand the regulatory mechanism of FoxO3a in early placental development.

# Methods And Materials

### Cell culture and cell knockdown

The cells involved in the experiment were immortalized human trophoblast HTR8/SVneo cell line obtained from the American Type Culture Collection (ATCC, Manassas, VA, USA) and incubated in the RPMI 1640 medium containing 10% fetal bovine serum（FBS, PAN, Germany）and 1% penicillin and streptomycin. The cells were cultured in a standard cultivation environment (in a humidified environment with 37℃ and 5% $CO_2$). Lentiviral vectors (GenePharma, China) were used to transfect HTR8/SVneo cells for 48 h to knock down the expression of FoxO3a, and there were two cell groups: control group (Normal) and scrambled shRNA group (sh-FoxO3a). Sodium nitroprusside (SNP) was selectively added into the complete medium to construct oxidative stress in the cells, and the optimal concentration has been explored in previous studies.

### Western blot

Cellular protein from the transfected HTR8/SVneo cells was extracted using RIPA lysis buffer (Beyotime Biotechnology, China) containing PMSF (1:100, Beyotime Biotechnology, China). The concentration of the extracted protein was determined by using a BCA assay kit (Beyotime Biotechnology, China). Each protein sample was loaded onto SDS-PAGE for electrophoresis and then transferred to a piece of PVDF membrane. TBST containing 5% skimmed milk was used to block the PVDF membrane for 1 h. Next, the membrane was incubated with various primary rabbit antibodies, including anti-FoxO3a (1:800, Catalog#:12829, Cell Signaling Technology) and β-actin (1:5000, Catalog#: GB11001, Servicebio) at 4 °C overnight. After incubated with goat anti-rabbit IgG for 1 h, bands density was detected using the Quantity One System image analyzer (Bio-Rad, USA).

### Cell migration assay

Wound Healing Assay was performed to assess the ability of migration between the normal group and the sh-FoxO3a group. $5´10^5$ cells were plated into a 6-well plate. A 200 μl sterile pipette tip was applied to scratch the cell monolayers when cells reached 90% confluence. Floating cells were removed with PBS, then cells remained were incubated in fresh complete mediums for 24 h. Images were taken by microscopy (EVOS FL Auto Imaging System, Life Technologies, USA) at the time point of 0h and 24 h after the scratch, and ImageJ software was used to measure the wound healing rate.

### Cell invasion assay

The invasiveness of the two group cells was detected using Matrigel invasion assay. After the diluted matrigel (BD BioScience) was added to the invasion chamber for 4 h, about $5´10^4$ cells were seeded into the upper compartment. After incubation for 24 h, a cotton swab was used to wipe the residual cells in the upper chamber. The lower chamber cells were fixed using 4% paraformaldehyde, washed with PBS, and stained using crystal violet (Beyotime Biotechnology, China). We used microscopy (EVOS FL Auto Imaging System, Life Technologies, USA) to determine the amount of the cells on the lower chamber. ImageJ software was used to evaluate the invasion rate.

### Metabolic flux analysis of the mitochondrial

Seahorse XFp Analyzer (Agilent, Santa Clara, CA) was used to evaluate the oxygen consumption rate (OCR), which reflected the mitochondrial function. HTR8/SVneo cells (Normal group, sh-FoxO3a group, Normal+SNP group, sh-FoxO3a+SNP group) were seeded in Seahorse XFp plates and cultured in a complete medium overnight. The next day, XF assay medium was added to replace the complete medium, and then the cells were incubated at 37℃ without $CO_2$ input atmosphere. FCCP (working concentration:10 mM), Oligomycin (working concentration: 2.5 mM), and Rotenone (working concentration: 0.5 mM) were added into the probe separately. At the time point of 26 min (basal respiration detection lasted for 26 min), 50 min and 70 min, oligomycin (2.5 mM), FCCP (10 mM), antimycin A (2.5 mM) /rotenone (2.5 mM) were injected into the chamber respectively. Mitochondrial parameters (basal respiration, proton spill, maximal respiration, and ATP turnover rate) were evaluated by various OCR indexes. Seahorse XFp software was used to analyze the OCR index.

### Intracellular, extracellular, and biomass metabolite extraction from cell culture

2 ml of each culture medium of normal and knockdown group HTR8/SVneo cells was used for extracellular chemical derivatization. For the intracellular metabolite extraction, 10 ml of liquid nitrogen was added to each plate of HTR8/SVneo cells. Then cold methanol/chloroform (9:1), containing the standard internal 2,3,3,3-d4-alanine (0.3 μmol), was used to extract metabolite from HTR8/SVneo cells. The collected samples were centrifuged at 15000 g for 15 min at 4℃, and the supernatant and the biomass were obtained. The supernatant attained was dried in the SpeedVac (Labconco Corp., Missouri, USA) for 5 h at room temperature and stored at -80℃ for intracellular chemical derivatization. For the biomass metabolite extraction, the fraction of biomass was dissolved in 100 ml sodium hydroxide, and then samples were kept at 98℃ for 10 min. 100 ml dd$H_2O$ and 200 ml methanol were added to each heated sample. The collected specimens were centrifuged at 15000 g for 15 min at 4℃, and the supernatant was obtained for chemical derivatization.

### Chemical derivatization of metabolites and GC-MS assay

The samples from Intracellular, extracellular, and biomass were derivatized using the methyl chloroformate (MCF) method as previously described (Smart et al. 2010). The chemical derivatives were analyzed by a system of Agilent GC7890B coupled to an MSD5977A mass selective detector (EI) set at 70 eV. The ZB-1701 GC capillary column (30 m × 250 μm id ×0.15 μm with 5 m guard column, Phenomenex) was used for metabolite analysis. The parameter analysis was previously described (Smart et al. 2010).

### GC-MS data analysis

The software, which is based on MassOmics XCMS R, was applied to extrapolate the relative abundance of the metabolites through the peak height of the most enriched ion mass (https://zenodo.org/record/4961895). Aiming to achieve stable repeatability and instrumental deviations and minimize sample preparation, the corresponding concentration of the identified metabolites normalized by an internal standard (D4-alanine), total ion concentration of the cellular metabolome, and revised by quality control of pooled samples. Before the HTR8/SVneo metabolome was analyzed, each metabolite concentration was transformed by log10 scale and Pareto scaling set up Gaussian distribution for this data. Model validation and partial least squares discriminant analysis (PLS-DA) were operated through MetaboAnalyst 5.0 (https://www.metaboanalyst.ca/). The Student's *t*-test and false discovery rate were implemented to calculate the significance of HTR8/SVneo metabolites between two groups by using R software. Only two-tailed *P*-values less than 0.05 were regarded as statistically significant. Receiver operating characteristic (ROC) curves were conducted using the pROC R package (Robin et al. 2011). Pathway enrichment analysis was performed by blasting our identified metabolites to the Kyoto Encyclopedia of Genes and Genomes (KEGG) database. The chord plot illustrated how the GOplot R package rendered metabolites participating in KEGG metabolic pathways.

### Isotope Tracer Experiment

The effect of 13C-labeled tracer (U-$^{13}C_6$ glucose) on flux estimation precision was measured in previous research (reference). There were two types of culture mediums used in $^{13}C$-glucose isotope labeling and metabolomics experiments: 1. RPMI 1640 medium containing 30% $^{13}C_6$-labelled glucose (U-$^{13}C_6$ glucose); 2. RPMI 1640 medium containing 30% $^{12}C_6$-labelled glucose. Subsequently, as described above, metabolite extraction, chemical derivatization, and GC-MS analysis were performed.

### Cellular oxidative stress detection

ROS in the HTR8/SVneo cells was measured using a ROS Detection Assay Kit (Beyotime, China). After knockdown of FoxO3a by lentiviral vectors (GenePharma, China) for 2 days, the HTR8/SVneo cells seeded in six-well plates were incubated with 1.5 mL of 0.1% DCFH-DA (diluted with a-MEM) at 37℃ for 25 min, and then complete medium-BSA free was used to wash the cells for three times. Subsequently, green fluorescence was evaluated by using a fluorescence microscope.

### RNA sequencing

According to the manufacturer's protocol, total RNA was extracted from HTR8/SVneo cells when it reached 90% fusion with TRIzol (Invitrogen, Carlsbad, CA, USA). Then, Agilent 2100 Bioanalyzer (Agilent Technologies, Palo Alto, CA, USA) was used to assess the quantity of RNA, and then qualified RNA was detected by performing agarose gel electrophoresis (RNase free). Next, beads of Oligo(dT) were applied to enrich mRNA. The enriched RNA fragments were broken by ultrasound and then as templates to synthesize cDNA with random primers. Before the purified cDNA came to Illumina, sequencing adapters, end-repaired, and poly(A) added were performed using a PCR extraction kit (Qiagen, Venlo, The Netherlands). RNase-free agarose gel electrophoresis was operated for size selection of the ligation products. Next, fragments amplified by PCR were sequenced using Illumina HiSeq2500 by Gene Denovo Biotechnology company (Guangzhou, China). Differential expression of the obtained RNA (two groups) was conculcated by DESeq2 and edgeR software. Only the false discovery rate (FDR) below 0.05 and fold change $\geq 2$ of these transcripts were considered differentially expressed genes.

### qRT-PCR

According to the manufacturer's instructions, RNA of the two groups of cultured cell lines was extracted using TRIzol reagent (Invitrogen, USA). The obtained RNA concentration was assessed using ultraviolet spectroscopy (Nano Drop 2000, Thermo, USA). Subsequently, Roche Reverse Transcription Kit (#07912455001, Roche, Germany) transcribes 1 mg RNA of each sample to cDNA reversely. GAPDH (housekeeping gene) was used to control relative gene expression analysis. The primer pairs of GAPDH were: forward: 5' GGAAGCTTGTCATCAATGGAAATC 3', reverse: 5' TGATGACCCTTTTGGCTCCC 3'. Primers for the target gene were as follows: COX-2: forward: 5' AAGACAGATCATAAGCGAGGGC 3', reverse: 5' AAACCGTAGATGCTCAGGGACT 3'; MMP9: forward: 5' TCGACGTGAAGGCGCAGAT 3', reverse: 5' AGAAGCGGTCCTGGCAGAAATA 3'.

# Results

### Depletion of the expression of FoxO3a in HTR8/SVneo cells.

The expression of FoxO3a was depleted by lentiviral transfection to explore how FoxO3a regulates the biological process and prepare for subsequent experiments. Our results demonstrated that the expression of FoxO3a was distinctly down-regulated in the knockdown group (Figure 1A).

### FoxO3a deletion inhibited the migration/invasion process of HTR8/SVneo cells.

We performed Wound Healing Assay and Matrigel cell invasion assay to investigate the effect of sh-FoxO3a on HTR8/SVneo cells. It was shown that the wound healing rate (the ability of migration, Figure 1B) and Matrigel cell invasion (the ability of invasion, Figure 1B) of the sh-FoxO3a group decreased compared with the normal group.

### Differences in intracellular metabolite and biomass profiles between the normal and sh-FoxO3a groups.

To explore how the FoxO3a gene influences metabolic changes, we compared the difference in intracellular metabolites and biomass between the control and knockdown groups. For intracellular metabolites, there were 347 GC-MS peaks detected in the normal group and sh-FoxO3a group, and 242 of which were identified by our MCF mass library. We used partial least square discriminant analysis (PLS-DA) to diversify the characteristics of the metabolic data of GC-MS, and the result revealed that the normal group and the sh-FoxO3a group were clustered separately (Figure 2A). The univariate analysis showed that 28 metabolites differed distinctly between the normal and sh-FoxO3a groups ($P < 0.05$; Figure 2B). The abundance of most metabolites increased in the sh-FoxO3a group, and only a few metabolites, including NADP_NADPH, Palmitoleic acid (C16_1n-7c), Benzoic acid, Itaconic acid, Decanoic acid (C10_0), and cis-Aconitic acid, decreased (Figure 2B). Changes in these metabolite ratios in two groups may likely result from the migration and invasion.

Interestingly, there were 16 metabolites under the receiver operating characteristic (ROC) curve was greater than 90%, including three organic acids, eight amino acids, one amino acid derivatives, two long-chain unsaturated fatty acids, one branched-chain unsaturated fatty acids, and one saturated fatty acid (Figure 2C). There were 89 GC-MS peaks detected in the two groups for biomass profiles, which our MCF mass library identified. PLS-DA was used to diversify the characteristics of the biomass data, and the result revealed that the normal group and the sh-FoxO3a group were clustered separately (Figure 3A). The univariate analysis illustrated that 31 metabolites differed distinctly between the normal and sh-FoxO3a groups ($P < 0.05$; Figure 3B). Almost all amino acids and long-chain fatty acids were down-regulated in the FoxO3a knockdown group.

### Differential concentration of extracellular metabolic profiles between the normal and sh-FoxO3a groups.

We further detected the metabolite differences in the medium to support our intracellular metabolic profile. The results were contrary to the trend of intracellular metabolite differences. We found that

FoxO3a knockout reduced extracellular secretion or promoted extracellular metabolites absorption, which is inconsistent with the intracellular findings. The above red line (positive values) indicates secretion, which means absorption below the red line (negative values). As we can see, tyrosine, phenylalanine, and tryptophan owned a lower concentration in the medium after FoxO3a depletion (Figure 3C).

**Effect of FoxO3a gene knockdown on the intracellular metabolic state of HTR8/SVneo cells.**

The R package of Pathway Activity Profiling (PAPi) was used to generate a metabolic activity profile based on the intracellular metabolites of the control and knockdown groups. It was shown that 11 metabolic pathways were significantly enriched, including

phenylalanine and tyrosine metabolism, tryptophan metabolism, tyrosine metabolism, catecholamine biosynthesis, methylhistidine metabolism, biotin metabolism, thyroid hormone synthesis, pyruvate metabolism, warburg effect, and alpha linolenic acid/linoleic acid metabolism ($P < 0.05$; Figure 2D). The result was represented to be in response to the gene FoxO3a deletion.

**The metabolite distribution profile of 30% $^{13}$C6-labelled glucose or 30% $^{12}$C6-labelled glucose is the only carbon source for HTR8/SVneo cells.**

To track how the knockdown of the gene FoxO3a affects the cell metabolism profile, we used $^{13}$C-labelled glucose as the only carbon source to provide cells in the control group and knockdown group. Our principle was that the labeled carbon atoms of a metabolite increase, proving that the labeled carbon source is converted to it. In short, the labeling metabolite owns a higher rate of biochemical conversion. As we can see, tyrosine, phenylalanine, and tryptophan owned a lower rate of biochemical conversion after FoxO3a depletion, while proline and succinate were contrary (Figure 4A).

**sh-FoxO3a restrained the respiration of HTR8/SVneo cells and elevated intracellular ROS.**

To investigate whether FoxO3a was involved in regulating mitochondrial respiration, we performed a seahorse assay to test the mitochondrial oxygen consumption rate (OCR). Compared to the normal group, the sh-FoxO3a group, normal + SNP group, and sh-FoxO3a+SNP group exhibited a distinct reduction in basal respiration and proton leak, which was reflected from decreased oxygen consumption (Figure 5A). For ATP production, only the group of sh-FoxO3a+SNP showed a significant loss versus the control group (Figure 5A). Under the condition of oxidative stress caused by SNP, both the control group and the knockdown group displayed a definite reduction in maximal respiration and non-mitochondrial oxygen consumption (Figure 5A). Therefore, we assumed that there was increased oxidative stress in the cells. We performed a ROS activity assay to investigate whether FoxO3a knockdown induced oxidative stress. The results showed that ROS accumulated in the cells after FoxO3a depletion (Figure 5B).

**The migration was the most differential biological process after sh-FoxO3a knockdown in HTR8/SVneo cells.**

To explore the potential molecular mechanism related to FoxO3a, we performed an RNA-Seq experiment. We found that many genes were upregulated or downregulated (Figure 6A). When we conducted GO enrichment analysis on these genes, we found that the most influential biological process was migration (Figure 6C). Subsequently, we performed correlation analysis between transcriptomics and metabolomics profiles, and we found nine genes positively correlated with significantly differential metabolites (Figure 6B). qRT-PCR unveiled that the expression of genes COX-2 (also called prostaglandin-endoperoxide synthase 2 (PTGS2)) and MMP9 were decreased (Figure 6D).

# Discussion

Our research was the first to apply transcriptomic, metabolomic, and isotope labeling experiments to explore the role of FoxO3a in regulating migration and invasion of trophoblast, which is essential for the early development of the placenta. Our data demonstrated that FoxO3a depletion restrained the migration and invasion of HTR8/SVneo cells. These phenotypical phenomena were also accompanied by the metabolic reprogramming of global metabolism and the utilization of extracellular nutrients such as aromatic amino acids and long-chain fatty acids. The migration/invasion process seems to be closely associated with metabolic remodeling and transcriptional reprogramming.

FoxO3a is a major contributing factor regulating energy metabolism through the switching between aerobic and anaerobic respiration. Metabolic flux (Figure 4A), seahorse (Figure 5A), and ROS analysis (Figure 5B) results showed that mitochondrial respiration was diminished along with reduced ATP production and excessive ROS. What is more, the concentration of lactic acid was elevated in response to the FoxO3a knockdown (Figure 2B). These findings implied that the knockdown of FoxO3a contributed to the impaired TCA cycle and the switch from oxidative phosphorylation toward glycolysis. Alessia Peserico et al. consistently reported that FoxO3a operated as a protection mechanism to maintain cellular respiration upon metabolic stress and nutrient shortage. Their research illustrated that a transcriptional complex (FoxO3a, SIRT3, and RNA polymerase at DNA regulatory regions of mitochondria) would be activated to protect mitochondrial respiration against oxidative stress (Peserico et al. 2013). It has also been reported that FoxO3a promoted the expression of the mitochondrial respiratory-related genome to facilitate aerobic respiration for ATP production (Celestini et al. 2018). On the other hand, our transcriptomic data revealed that FoxO3a knockdown reduced the expression of hexokinase domain containing 1 (HKDC1), which is known to suppress gluconeogenesis (IrwinTan 2008). Khan *et al.* also demonstrated that hepatic HKDC1 overexpression upon pregnancy reduces gluconeogenesis in mice (Khan et al. 2019; Zapater et al. 2021). Gluconeogenesis seems to be upregulated to fulfill the energy demand by utilizing alternative substracts to compensate for the inhibition of mitochondrial respiration by Foxo3a. It could be a potential reason that aromatic amino acids and long-chain fatty acids were uptaken from their external environment. Thus, there was a metabolic shift from oxidative phosphorylation to glycolysis along with elevated gluconeogenesis after FoxO3a knockdown.

FoxO3a-mediated migration/invasion of trophoblast seem to be associated with aromatic amino acid and long-chain fatty acid metabolism in early pregnancy. We found that the migration and invasion of

HTR8/SVneo cells were compromised after FoxO3a knockdown (Figure 1). Our intracellular metabolites (Figure 2), extracellular metabolites (Figure 3C), biomass (Figure 3B), and $^{13}C$-labelled glucose metabolic flux (Figure 4A) results showed that there were many significantly differential enrichments of amino acids between wildtype and FoxO3a knockdown, particularly aromatic amino acids were accumulated in level and reduced $^{13}C$ flux enrichment intracellularly. Recently, several researchers reported that tryptophan (one of the three aromatic amino acids) had been involved in migration and invasion via cyclooxygenase-2 (COX-2, also named PTGS2) and matrix metallopeptidase 9 (MMP9) (Gu et al. 2021; Liu et al. 2020). Our previous RNA-seq study consistently demonstrated that the expressions of COX-2 and MMP9 were decreased after FoxO3a depletion (27), and the expression of these two genes is negatively correlated with all three aromatic amino acids acid concentrations under FoxO3a knockdown condition (Figure 6B). Moreover, it has been proposed that melatonin and 5-methoxytryptophan (5-MTP) are downstream metabolites from tryptophan that abrogated P52 binding to κB enhancer elements at COX-2 promoters, thereby inhibiting the COX-2 expression (Cheng et al. 2012; Deng et al. 2006; Wu et al. 2014). Furthermore, COX-2 is a rate-limiting enzyme that mediates the production of prostaglandin E2 (PGE2) from arachidonic acid (AA). Subsequently, PGE2 activates JAK2/STAT3 pathway to elevate the expression of metallopeptidase 9 (MMP9) (Kawahara et al. 2015; Lee et al. 2020). On the other hand, our intracellular profiles (Figure 2) showed that many long-chain fatty acids (e.g., arachidonic acid and a-Linolenic acid) were accumulated inside the HTR8/SVneo cells. Although there was no significant difference of arachidonic acid (AA) between wildtype and knockdown group in intracellular metabolite profile, the ratio of AA to linolenic acid (a metabolite upstream of AA) and the abundance of adrenic acid (a metabolite downstream of AA) increased compared to the normal group. Recently, a-Linolenic acid (ALA) was reported to suppress migration and invasion in many malignant tumors, such as prostate (du Toit et al. 1996), colon (ChamberlandMoon 2015), and breast (Wiggins et al. 2015). Another study showed that ALA could inhibit cell migration and invasion via decreased expression of COX-2 that mediated the transformation of AA to prostaglandin E2 (PGE2) and then promoted MMP9-mediated migration and invasion (Deshpande et al. 2016). Our RNA-seq analysis illustrated that the expression of COX-2 and MMP9 were inhibited after FoxO3a depletion (Figure 6A), which may lead to compromise migration and invasion progress via impairing AA metabolism. Therefore, through transcriptomics and metabolomics, we suggested that FoxO3a depletion leads to the accumulation of intracellular aromatic acids and the long-chain fatty acid and subsequently may result in the inhibition of COX-2 and MMP9 mediated migration and invasion of trophoblast.

Aromatic amino acids may promote catecholamine anabolism and eventually contribute to placental oxidative stress. Our metabolic pathway analysis pinpointed that intracellular metabolic flux redirected aromatic amino acids toward catecholamine metabolism (Figure 2D). In the meanwhile, there was excessive ROS accumulated in the cells (Figure 5B). It is widely accepted that catecholamine is biosynthesized from phenylalanine and tyrosine (Nazari et al. 2020; Végh et al. 2016). There is also evidence that the placenta could synthesize catecholamine from aromatic amino acids, and the abundance of catecholamine in the preeclampsia was significantly increased compared to the normal pregnancy (Turner et al. 2008).

Moreover, the accumulation of catecholamine has been reported to elevate oxygen demand/supply imbalance, blood flow reduction, direct toxic effect, free radical formation, and increased excitotoxicity (Ma et al. 2004), which are the common pathophysiology observed in the dysregulated placenta. With the elevation of phenylalanine, tyrosine, and downstream metabolites, there was less blood and oxygen supply in the placenta, which may partly contribute to the trophoblast's poor migration/invasion. Thus, the underlying mechanisms of FoxO3a induced aromatic amino acid-catecholamine metabolism should be investigated in early placental development.

# Conclusions

In light of our study, we unmasked a novel role of FoxO3a in the metabolic remodeling and transcriptional reprogramming of early placental development, as illustrated in Figure 7. FoxO3a exerts an essential effect on trophoblast migration and invasion owing to the regulations of COX2, MMP9, aromatic amino acids, energy metabolism, and oxidative stress. Future studies should elucidate how FoxO3a mechanistically maneuvers the underlying metabolic alternations.

# Abbreviations

FoxO3a: forkhead box O3a protein; GC-MS: gas-chromatography-mass spectrometry; PE: preeclampsia FGR: fetal growth restriction; Foxes: forkhead protein factor family; AA: arachidonic acid; COX-2: Cyclooxygenase-2; PGE2: prostaglandin E2; SNP: Sodium nitroprusside; MCF: methyl chloroformate; PLS-DA: partial least squares discriminant analysis; ROC: Receiver operating characteristic; KEGG: Kyoto Encyclopedia of Genes and Genomes; FDR: false discovery rate; PAPi: Pathway Activity Profiling; OCR: oxygen consumption rate; PTGS2: prostaglandin-endoperoxide synthase 2; HKDC1: hexokinase domain containing 1; MMP9: matrix metallopeptidase 9; 5-MTP: 5-methoxytryptophan; ALA: a-Linolenic acid.

# Declarations


### Acknowledgments

This work was supported by the National Natural Science Foundation of China (No. 81971406, 81771607, 81871185, 81901507, 81961128004), The 111 Project (Yuwaizhuan (2016)32), Chongqing Health Commission (2018ZDXM024), Chongqing Health Commission and Chongqing Science & Technology Commission (2021MSXM121, 2020MSXM101, KJZD-K202100407)


### Authors' contributions

HC, SHW, and TLH performed the research; HC, SHW, TLH, and HZ interpreted and analyzed the data; HC, SHW, TLH, HZ, CC, XYY, JNZ, TM, BN, RF, and PB reviewed and edited the manuscript; HC, SHW, TLH, and HZ wrote the manuscript. HC, HZ, and TLH were responsible for conception and design of the project. HZ and TLH was responsible for supervision and project administration.

### Funding

The National Natural Science Foundation of China (No. 81971406, 81771607, 81871185, 81901507, 81961128004), The 111 Project (Yuwaizhuan (2016)32), Chongqing Health Commission (2018ZDXM024), Chongqing Health Commission and Chongqing Science & Technology Commission (2021MSXM121, 2020MSXM101, KJZD-K202100407)

### Availability of data and materials

All of the data generated in this study are illustrated in this article.

### Ethics approval and consent to participate

Not applicable.

### Consent for publication

Not applicable.

### Competing interests

There are no competing interests.

# References

1. Amrit F, Steenkiste E, Ratnappan R, Chen S, McClendon T, Kostka D, Yanowitz J, Olsen C, Ghazi A. DAF-16 and TCER-1 Facilitate Adaptation to Germline Loss by Restoring Lipid Homeostasis and Repressing Reproductive Physiology in C. elegans. PLoS genetics. 2016;12(2):e1005788. doi:10.1371/journal.pgen.1005788.
2. Brosens I, Pijnenborg R, Vercruysse L, Romero R. The “Great Obstetrical Syndromes” are associated with disorders of deep placentation. American Journal of Obstetrics Gynecology. 2011;204(3):193–201. doi:10.1016/j.ajog.2010.08.009.
3. Burton GJ, Watson AL, Hempstock J, Skepper JN, Jauniaux E. Uterine glands provide histiotrophic nutrition for the human fetus during the first trimester of pregnancy. J Clin Endocrinol Metab. 2002;87(6):2954–9. doi:10.1210/jcem.87.6.8563.
4. Carlsson P, Mahlapuu M. Forkhead transcription factors: key players in development and metabolism. Dev Biol. 2002;250(1):1–23. doi:10.1006/dbio.2002.0780.
5. Celestini V, Tezil T, Russo L, Fasano C, Sanese P, Forte G, Peserico A, Lepore Signorile M, Longo G, De Rasmo D, Signorile A, Gadaleta R, Scialpi N, Terao M, Garattini E, Cocco T, Villani G, Moschetta A, Grossi V, Simone C. Uncoupling FoxO3A mitochondrial and nuclear functions in cancer cells undergoing metabolic stress and chemotherapy. Cell death disease. 2018;9(2):231. doi:10.1038/s41419-018-0336-0.

6. Chamberland J, Moon H. Down-regulation of malignant potential by alpha linolenic acid in human and mouse colon cancer cells. Familial cancer. 2015;14(1):25–30. doi:10.1007/s10689-014-9762-z.
7. Cheng H, Kuo C, Yan J, Chen H, Lin W, Wang K, Tsai K, Guvén H, Flaberg E, Szekely L, Klein G, Wu K. Control of cyclooxygenase-2 expression and tumorigenesis by endogenous 5-methoxytryptophan. Proceedings of the National Academy of Sciences of the United States of America. 2012;109(33):13231–6. doi:10.1073/pnas.1209919109.
8. Cui P, Rawling T, Bourget K, Kim T, Duke C, Doddareddy M, Hibbs D, Zhou F, Tattam B, Petrovic N, Murray M. Antiproliferative and antimigratory actions of synthetic long chain n-3 monounsaturated fatty acids in breast cancer cells that overexpress cyclooxygenase-2. Journal of medicinal chemistry. 2012;55(16):7163–72. doi:10.1021/jm300673z.
9. Dansen T, Kops G, Denis S, Jelluma N, Wanders R, Bos J, Burgering B, Wirtz K. Regulation of sterol carrier protein gene expression by the forkhead transcription factor FOXO3a. Journal of lipid research. 2004;45(1):81–8. doi:10.1194/jlr.M300111-JLR200.
10. Deng W, Tang S, Tseng H, Wu K. Melatonin suppresses macrophage cyclooxygenase-2 and inducible nitric oxide synthase expression by inhibiting p52 acetylation and binding. Blood. 2006;108(2):518–24. doi:10.1182/blood-2005-09-3691.
11. Deshpande R, Mansara P, Kaul-Ghanekar R. Alpha-linolenic acid regulates Cox2/VEGF/MAP kinase pathway and decreases the expression of HPV oncoproteins E6/E7 through restoration of p53 and Rb expression in human cervical cancer cell lines. Tumour biology: the journal of the International Society for Oncodevelopmental Biology Medicine. 2016;37(3):3295–305. doi:10.1007/s13277-015-4170-z.
12. du Toit P, van Aswegen C, du Plessis D. The effect of essential fatty acids on growth and urokinase-type plasminogen activator production in human prostate DU-145 cells. Prostaglandins leukotrienes essential fatty acids. 1996;55(3):173–7. doi:10.1016/s0952-3278(96)90094-0.
13. Gu K, Liu G, Wu C, Jia G, Zhao H, Chen X, Tian G, Cai J, Zhang R, Wang J. Tryptophan improves porcine intestinal epithelial cell restitution through the CaSR/Rac1/PLC-γ1 signaling pathway. Food function. 2021. doi:10.1039/d1fo01075a.
14. Hasim A, Aili A, Maimaiti A, Mamtimin B, Abudula A, Upur H. Plasma-free amino acid profiling of cervical cancer and cervical intraepithelial neoplasia patients and its application for early detection. Molecular biology reports. 2013;40(10):5853–9. doi:10.1007/s11033-013-2691-3.
15. Hasim A, Ma H, Mamtimin B, Abudula A, Niyaz M, Zhang L, Anwer J, Sheyhidin I. Revealing the metabonomic variation of EC using $^{1}$H-NMR spectroscopy and its association with the clinicopathological characteristics. Molecular biology reports. 2012;39(9):8955–64. doi:10.1007/s11033-012-1764-z.
16. Hedrick SM, Hess Michelini R, Doedens AL, Goldrath AW, Stone EL. FOXO transcription factors throughout T cell biology. Nat Rev Immunol. 2012;12(9):649–61. doi:10.1038/nri3278.
17. Hemberger M, Hanna CW, Dean W. Mechanisms of early placental development in mouse and humans. Nat Rev Genet. 2020;21(1):27–43. doi:10.1038/s41576-019-0169-4.

18. Irwin D, Tan H. Molecular evolution of the vertebrate hexokinase gene family: Identification of a conserved fifth vertebrate hexokinase gene. Comparative biochemistry physiology Part D Genomics proteomics. 2008;3(1):96–107. doi:10.1016/j.cbd.2007.11.002.
19. Kawahara K, Hohjoh H, Inazumi T, Tsuchiya S, Sugimoto Y. Prostaglandin E2-induced inflammation: Relevance of prostaglandin E receptors. Biochimica et biophysica acta. 2015;1851(4):414–21. doi:10.1016/j.bbalip.2014.07.008.
20. Khan M, Priyadarshini M, Cordoba-Chacon J, Becker T, Layden B. Hepatic hexokinase domain containing 1 (HKDC1) improves whole body glucose tolerance and insulin sensitivity in pregnant mice. Biochimica et biophysica acta Molecular basis of disease. 2019;1865(3):678–87. doi:10.1016/j.bbadis.2018.11.022.
21. Lee T, Liu P, Tsai M, Chen J, Wang S, Hsieh H. The COX-2-derived PGE autocrine contributes to bradykinin-induced matrix metalloproteinase-9 expression and astrocytic migration via STAT3 signaling. Cell communication signaling: CCS. 2020;18(1):185. doi:10.1186/s12964-020-00680-0.
22. Liu L, Ma Z, Zhou X, Yin J, Lu J, Su J, Shen F, Xie L, Hu S, Ling J. Tryptophan 387 and 390 residues in ADAMTS13 are crucial to the ability of vascular tube formation and cell migration of endothelial cells. Clinical experimental pharmacology physiology. 2020;47(8):1402–9. doi:10.1111/1440-1681.13313.
23. Ma D, Rajakumaraswamy N, Maze M. alpha2-Adrenoceptor agonists: shedding light on neuroprotection? British medical bulletin. 2004;71:77–92. doi:10.1093/bmb/ldh036.
24. Nazari M, Rosenblum J, Haigney M, Rosing D, Pacak K. Pathophysiology and Acute Management of Tachyarrhythmias in Pheochromocytoma: JACC Review Topic of the Week. Journal of the American College of Cardiology. 2020;76(4):451–64. doi:10.1016/j.jacc.2020.04.080.
25. Peserico A, Chiacchiera F, Grossi V, Matrone A, Latorre D, Simonatto M, Fusella A, Ryall J, Finley L, Haigis M, Villani G, Puri P, Sartorelli V, Simone C. A novel AMPK-dependent FoxO3A-SIRT3 intramitochondrial complex sensing glucose levels. Cellular molecular life sciences: CMLS. 2013;70(11):2015–29. doi:10.1007/s00018-012-1244-6.
26. Robin X, Turck N, Hainard A, Tiberti N, Lisacek F, Sanchez J, Müller M. pROC: an open-source package for R and S+ to analyze and compare ROC curves. BMC bioinformatics. 2011;12:77. doi:10.1186/1471-2105-12-77.
27. Smart K, Aggio R, Van Houtte J, Villas-Bôas S. Analytical platform for metabolome analysis of microbial cells using methyl chloroformate derivatization followed by gas chromatography-mass spectrometry. Nature protocols. 2010;5(10):1709–29. doi:10.1038/nprot.2010.108.
28. Szymczak M, Murray M, Petrovic N. Modulation of angiogenesis by omega-3 polyunsaturated fatty acids is mediated by cyclooxygenases. Blood. 2008;111(7):3514–21. doi:10.1182/blood-2007-08-109934.
29. Turner E, Brewster J, Simpson N, Walker J, Fisher J. Aromatic amino acid biomarkers of preeclampsia–a nuclear magnetic resonance investigation. Hypertension in pregnancy. 2008;27(3):225–35. doi:10.1080/10641950801955725.

30. Végh A, Duim S, Smits A, Poelmann R, Ten Harkel A, DeRuiter M, Goumans M, Jongbloed M. Part and Parcel of the Cardiac Autonomic Nerve System: Unravelling Its Cellular Building Blocks during Development. Journal of cardiovascular development disease 2016; 3(3). doi:10.3390/jcdd3030028.
31. Warr MR, Binnewies M, Flach J, Reynaud D, Garg T, Malhotra R, Debnath J, Passegue E. FOXO3A directs a protective autophagy program in haematopoietic stem cells. Nature. 2013;494(7437):323–7. doi:10.1038/nature11895.
32. Wiggins A, Kharotia S, Mason J, Thompson L. α-Linolenic Acid Reduces Growth of Both Triple Negative and Luminal Breast Cancer Cells in High and Low Estrogen Environments. Nutrition cancer. 2015;67(6):1001–9. doi:10.1080/01635581.2015.1053496.
33. Wu K, Cheng H, Chang T. 5-methoxyindole metabolites of L-tryptophan: control of COX-2 expression, inflammation and tumorigenesis. Journal of biomedical science. 2014;21:17. doi:10.1186/1423-0127-21-17.
34. Xu Y, Wu D, Jiang Z, Zhang Y, Wang S, Ma Z, Hui B, Wang J, Qian W, Ge Z, Sun L. MiR-616-3p modulates cell proliferation and migration through targeting tissue factor pathway inhibitor 2 in preeclampsia. Cell Prolif. 2018;51(5):e12490. doi:10.1111/cpr.12490.
35. Yang Y, Abdulhasan M, Awonuga A, Bolnick A, Puscheck EE, Rappolee DA. Hypoxic Stress Forces Adaptive and Maladaptive Placental Stress Responses in Early Pregnancy. Birth Defects Res. 2017;109(17):1330–44. doi:10.1002/bdr2.1149.
36. Zaheer A, Sahu S, Ryken T, Traynelis V. Cis-parinaric acid effects, cytotoxicity, c-Jun N-terminal protein kinase, forkhead transcription factor and Mn-SOD differentially in malignant and normal astrocytes. Neurochemical research. 2007;32(1):115–24. doi:10.1007/s11064-006-9236-2.
37. Zapater J, Lednovich K, Layden B. The Role of Hexokinase Domain Containing Protein-1 in Glucose Regulation During Pregnancy. Current diabetes reports. 2021;21(8):27. doi:10.1007/s11892-021-01394-4.
38. Zhang W, Patil S, Chauhan B, Guo S, Powell DR, Le J, Klotsas A, Matika R, Xiao X, Franks R, Heidenreich KA, Sajan MP, Farese RV, Stolz DB, Tso P, Koo SH, Montminy M, Unterman TG. FoxO1 regulates multiple metabolic pathways in the liver: effects on gluconeogenic, glycolytic, and lipogenic gene expression. J Biol Chem. 2006;281(15):10105–17. doi:10.1074/jbc.M600272200.

# Figures

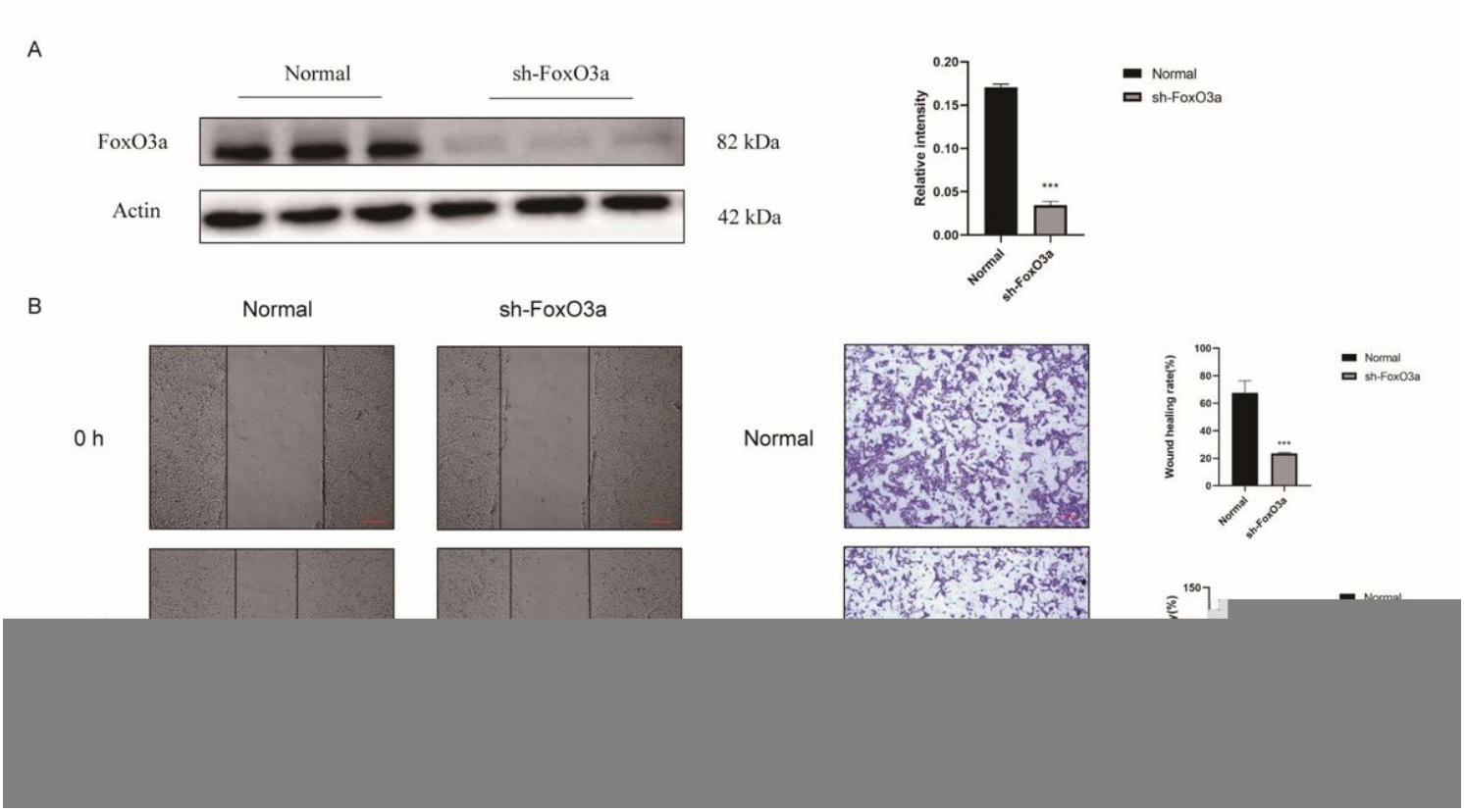


## Figure 1

**Detection of transfection efficiency of lentivirus targeting FoxO3a in HTR8/SVneo cells and the abilities of migration and invasion of HTR8/SVneo cells after FoxO3a depletion.** (A) After 48h transfection of lentivirus, the expression of FoxO3a in HTR8/SVneo cells was analyzed by Western Blot. (B) Wound-healing assay and Matrigel transwell assay illustrated migration and invasion abilities after FoxO3a depletion. Results are shown as mean ± SEM, n=3, $^{**}P < 0.01$ and $^{***}P < 0.001$.

## Figure 2

**The characteristics of the intracellular metabolic data.** (A) partial least square discriminant analysis (PLS-DA) between normal group and sh-FoxO3a group. (B)The student t-test analysis showed that 28 metabolites differed between the normal and knockdown groups. (C) The area under the receiver operating characteristic (ROC) curve for intracellular metabolites. There were 12 metabolites with the area under the ROC curve greater than 90%, mainly amino acids and long-chain unsaturated fatty acids. (D) The R package of PAPi. Only statistically significant differences in metabolites and low false discovery rate ($P < 0.05$ by the Student's *t*-test) are illustrated.

## Figure 3

**The characteristics of the biomass and the extracellular metabolic data.** (A) PLS-DA between normal group and sh-FoxO3a group. (B) The Student's *t*-test analysis showed that 20 metabolites differed between the normal and the knockdown groups. (C) Extracellular metabolites difference between normal group and sh-FoxO3a group. Above the red line (positive values) indicates secretion; below (negative values) means absorption. Only statistically significant differences in metabolites and low false discovery rate (P < 0.05 by the Student's *t*-test) are illustrated.

## Figure 4

**$^{13}$C-labelled glucose metabolic flux and intracellular long-chain unsaturated fatty acids metabolism differences and Bioenergetics by Seahorse XFp metabolic flux analysis.** (A) Tyrosine, phenylalanine, and tryptophan owned a lower rate of biochemical conversion after FoxO3a depletion. (B) Our intracellular metabolic result showed differences in long-chain unsaturated fatty acids between normal and knockdown groups, and differential metabolites mostly belong to omega-6 or omega-3 fatty acids. Omega-3 and omega-6 fatty acids are mainly involved in inflammation and migration progress. Results are shown as mean ± SEM, n=3, $^{**}P < 0.01$ and $^{***}P < 0.001$.

## Figure 5

**Bioenergetics by Seahorse XFp metabolic flux analysis and the oxidative stress analysis.** (A) FoxO3a depletion group exhibited a distinct reduction in basal respiration and proton leak. (B) FoxO3a knockdown-induced oxidative stress. Intracellular ROS was measured by DCFH-DA staining (Scale bar = 400 um) and DCFH-DA fluorescence intensity. Results are shown as mean ± SEM, n=3, $^{**}P < 0.01$ and $^{***}P < 0.001$.

## Figure 6

**FoxO3a regulates HTR8/SVneo cells migration progress.** (A) The heatmap illustrates the copy numbers of mRNAs. Red represents higher transcription, and the green represents lower transcription. (B) Enriched Gene Ontology (GO) analysis illustrated that migration of HTR8/SVneo cells was the most affected biological process after FoxO3a exhaustion. (C) Correlation analysis between transcriptomics and metabolomics. Red represents positive correlation, and blue represents negative correlation. (D) qPCR shows reduced expression of the genes (COX-2 and MMP9). Only the results showing statistically significant Student's t-test ($P < 0.05$) and minimum false discovery rate (q < 0.05) are shown, n=3, $^{**}P < 0.01$ and $^{***}P < 0.001$.

## Figure 7

FoxO3a plays a role in metabolic remodeling and transcriptional reprogramming.